

# The *Multitaper* Spectrum Analysis Package in Python

Germán A. Prieto\*<sup>1</sup> 

## Abstract

Spectral analysis has been a fundamental tool in analyzing seismic signals for studying the earthquake source, propagation of seismic waveforms through the Earth, and even monitoring changes in Earth's structure. I present an open-source Python package, *multitaper*, for spectral analysis using the multitaper algorithm. The package not only includes power spectral density estimation (with confidence intervals) but also includes bivariate problems such as coherence, dual-frequency correlations, and deconvolution estimation. Implementation of the sine and quadratic multitaper algorithms is also available. For the reader to quickly learn how to use the package, I briefly present several examples using earthquake records from the 2019  $M_w$  6.0 Mesetas, Colombia, earthquake and its aftershocks recorded at regional distances for estimating time–frequency spectrograms, spectral ratio and source time functions, and correlations between neighboring frequencies. Jupyter Notebooks are shared to reproduce the figures.

**Cite this article as** Prieto, G. A. (2022). The *Multitaper* Spectrum Analysis Package in Python, *Seismol. Res. Lett.* **XX**, 1–8, doi: [10.1785/0220210332](https://doi.org/10.1785/0220210332).

## Introduction

Spectral analysis is a fundamental tool for the analysis of time and spatial series in geophysics (Båth, 1974; Tary *et al.*, 2014; Dannemann Dugick *et al.*, 2021). The objective of spectral analysis is the characterization of a time (or space) series, that is, to quantitatively say (1) what its frequency content is, (2) how one series differs from another, or (3) how two series are related. These three aspects are described in the frequency domain using the power spectral density (PSD), the spectral coherency, and the transfer (or frequency response) functions, respectively, or their time domain counterparts the autocovariance, the cross-correlation, and the impulse response (Percival and Walden, 1993; Bracewell, 2000).

Recent seismological applications of spectral analysis and the use of the functions listed earlier are broad, including earthquake source estimation (Madariaga *et al.*, 2019; Chaves *et al.*, 2020; Trugman and Savvaidis, 2021), attenuation tomography (Jang *et al.*, 2019), crust and mantle structure (Cossette *et al.*, 2016; Liu *et al.*, 2018), characterizing Global Navigation Satellite System sensors and ambient noise (Qin *et al.*, 2019; Melgar *et al.*, 2020a,b), array and Large-N seismology (Gibbons *et al.*, 2017; Kemna *et al.*, 2020), seismic interferometry, and structural health monitoring (Kong *et al.*, 2018; Bonilla *et al.*, 2019; Häusler *et al.*, 2021; Morelli *et al.*, 2021, and much more).

Methods for estimation of the spectrum include parametric and nonparametric methods. The first method (Olafsson and Sigbjörnsson, 1995; Diagourtas *et al.*, 2002; Ugalde *et al.*, 2021) is generally approached using autoregressive models (AR and similar) but is not the focus of this contribution.

The second method (the focus of this contribution) usually employs the fast Fourier transform of a discretely sampled data set after applying a taper (windowing). This approach is computationally efficient but comes with its limitations; the frequency resolution is bounded by the data length, and it suffers from spectral leakage—the tendency for energy from distant frequencies to appear in the frequency of interest (Kay and Marple, 1981; Prieto *et al.*, 2007). In addition, the variance of the spectrum estimate is large and, in many cases, averaging of nearby frequencies is required.

The multitaper algorithm first proposed by Thomson (1982) addresses this trade-off between bias and variance. It aims at reducing the bias by tapering using the orthogonal Slepian sequences that are constructed to optimally reduce spectral leakage and, as its name suggests, multiple independent estimates of the spectrum are averaged to reduce variance.

There are already several freely available codes that implement the multitaper algorithm in Fortran 77 (Pardo-Igúzquiza *et al.*, 1994), Julia (Haley and Geoga, 2020), R (Rahim *et al.*, 2014), C (Lees and Park, 1995), and Fortran 90 (Prieto *et al.*, 2009). Python implementations or wrapper of some of these codes include pymutt and mtspec (see [Data and Resources](#)), and the latter providing most features to the ones available here. The *multitaper* package (this contribution) is a

1. Departamento de Geociencias, Universidad Nacional de Colombia, Bogotá, Colombia,  <https://orcid.org/0000-0001-8538-7379> (GAP)

\*Corresponding author: gaprietogo@unal.edu.co

© Seismological Society of America

translation of the Fortran 90 (Prieto *et al.*, 2009) codes in Python and provides a unified platform for spectral analysis. It creates a Python class (*MtSpec*) with the resulting multitaper estimate of the PSD but can provide further information including confidence intervals, line detection, quadratic inverse PSD, and so on. In the case of studying two time series, another Python class (*MTCross*) is used. Unique features in this package include bivariate dual-frequency coherence and cross-correlations. In the following, I will provide three seismological examples on the use of *multitaper*. Jupyter Notebooks to reproduce the figures in this article and those of Prieto *et al.* (2009) are made available.

## Multitaper Spectrum Analysis

The multitaper algorithm is similar to other nonparametric spectral estimates in that the  $N$ -long time sequence  $y_n$  studied ( $n = 0, 1, \dots, N$ ) is multiplied by the  $k$ th taper  $v_k$  and then Fourier transformed

$$Y_k = \sum_{n=0}^{N-1} y_n v_k e^{-2\pi i f n}, \quad (1)$$

but instead of using a single taper, a  $K$  number of orthogonal tapers are applied such that the PSD estimate  $\hat{S}$  is

$$\hat{S}_y(f) = \frac{\sum_{k=0}^{K-1} w_k |Y_k(f)|}{\sum_{k=0}^{K-1} w_k}, \quad (2)$$

a weighted average of the  $Y_k$ s, in which the  $w_k$  are weights designed to reduce the spectral leakage while keeping the variance of the estimate low (see Thomson, 1982; Prieto *et al.*, 2009). The choice of weights  $w_k$  can be selected based on the eigenvalues of the tapers or using an adaptive weighting (Thomson, 1982). The quadratic multitaper estimate (Prieto *et al.*, 2007) uses the second derivative of the spectrum to obtain a higher resolution estimate of the spectrum.

When working with two time series  $x$  and  $y$ , and for simplicity assuming  $w_k = 1$  the estimate of the cross-spectrum is

$$\hat{S}_{xy}(f) = \sum_{k=0}^{K-1} X_k(f) Y_k^*(f), \quad (3)$$

and the coherence and transfer functions are

$$\hat{C}_{xy}(f) = \frac{S_{xy}(f)}{\sqrt{S_x(f)} \sqrt{S_y(f)}}, \quad (4)$$

$$\hat{T}_{xy}(f) = \frac{S_{xy}(f)}{S_y(f)}. \quad (5)$$

The squared of  $C_{xy}$  is called the squared coherence and has values between 0 and 1 and represents the similarity of the two waveforms (it is analogous to the cross-correlation). The *multitaper* allows the user the inverse Fourier transform on these three

estimates to obtain the cross-correlation, normalized cross-correlation, and the deconvolution between the two signals.

For nonstationary signals, the spectra at distant frequencies are correlated (Thomson and Vernon, 1998; Larsen and Hanssen, 2004; Prieto *et al.*, 2005). The dual-frequency coherence (DFC)—a matrix of spectral coherence between frequencies ( $f_1, f_2$ )—can be estimated as

$$\hat{C}_{xy}(f_1, f_2) = \frac{\sum_{k=0}^{K-1} X_k(f_1) Y_k^*(f_2)}{\sqrt{S_x(f_1)} \sqrt{S_y(f_2)}}. \quad (6)$$

If the DFC is estimated for a single time series, the main diagonal of the matrix ( $f_1 = f_2$ ) has unit amplitude, while the off-diagonal term's amplitudes will depend on the nature of the signal (diffusive, nonstationarity, etc.). If the DFC is estimated for two distinct time series, the main diagonal represents the coherence (as in equation 4). The off-diagonal terms reflect the correlation between the spectra at distant frequencies, for example, for dispersive or diffusive signals (see examples in Mellors *et al.*, 1998; Prieto *et al.*, 2005; Liu and Ben-Zion, 2016, 2018; Liu and Beroza, 2020).

## Data

In this work, three examples using seismological data are presented. All examples use records of the  $M_w$  6.0 Mesetas earthquake and its aftershocks (Mayorga *et al.*, 2020; Noriega-Londoño *et al.*, 2021) on 24 December 2019, recorded at regional distances by stations from the Servicio Geológico Colombiano (SGC) and a temporary deployment inside a 14-story building in downtown Bogota (Jaimes *et al.*, 2022). The 2019  $M_w$  6.0 Mesetas earthquake was followed by an  $M_w$  5.8 aftershock just 15 min later (see Fig. 1). In the following months at least 20  $M_w$  4+ earthquakes were located in the mainshock area (see Data and Resources).

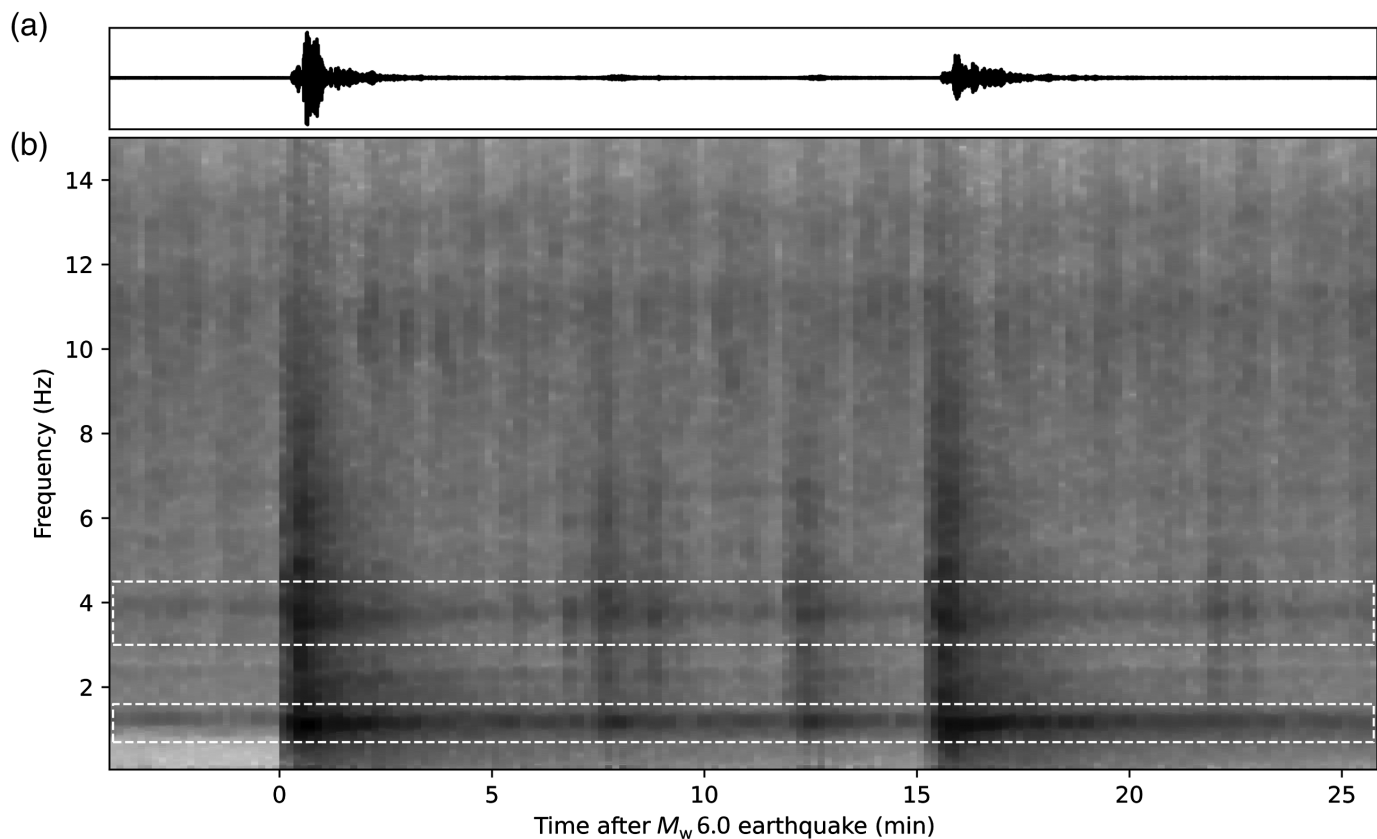
## Time Varying Response of a Building

Figure 1 shows the recorded ground motions of the horizontal component at the 14th floor of the Crisanto building in downtown Bogota (Jaimes *et al.*, 2022). Both the  $M_w$  6.0 and  $M_w$  5.8 earthquakes are clearly visible and some  $M_w$  4+ in between are also evident. The time–frequency spectrogram shown is calculated for 20-s-long windows with a 50% overlap using the adaptive and quadratic multitaper estimates (see pseudo-code 1):

### Pseudo-code 1 - Spectrogram

```
import multitaper.mtspec as spec
t,freq,qi,adap = spec.spectrogram(x,dt,twin=20.,olap=0.5,
nw,kspec)
```

in which  $x$  is the entire trace shown in Figure 1,  $nw$ ,  $kspec$ , and  $dt$  are the time-bandwidth product, the number of tapers to use, and the sampling rate, respectively, and  $twin$  and  $olap$  show the function of the length of each window and the proportion of



overlap for constructing the spectrogram. The function returns the time and frequency vectors  $t$ ,  $freq$  and the quadratic and adaptive spectrum estimates  $qi$ ,  $adap$ .

For each 20 s window, the function calls the multitaper modules (pseudo-code 2):

#### Pseudo-code 2 – Individual spectra

```
from multitaper import MTSpec
psd = MTSpec(y,nw,kspec,dt)
freq = psd.freq
adap0 = psd.spec
qi0 = psd.qiinv()[0]
```

in which  $y$  is the 20 s waveform (cut from the entire trace). The adaptive spectrum  $adap0$  as well as the quadratic estimate  $qi0$  for a single window can be requested from the  $psd$  variable.

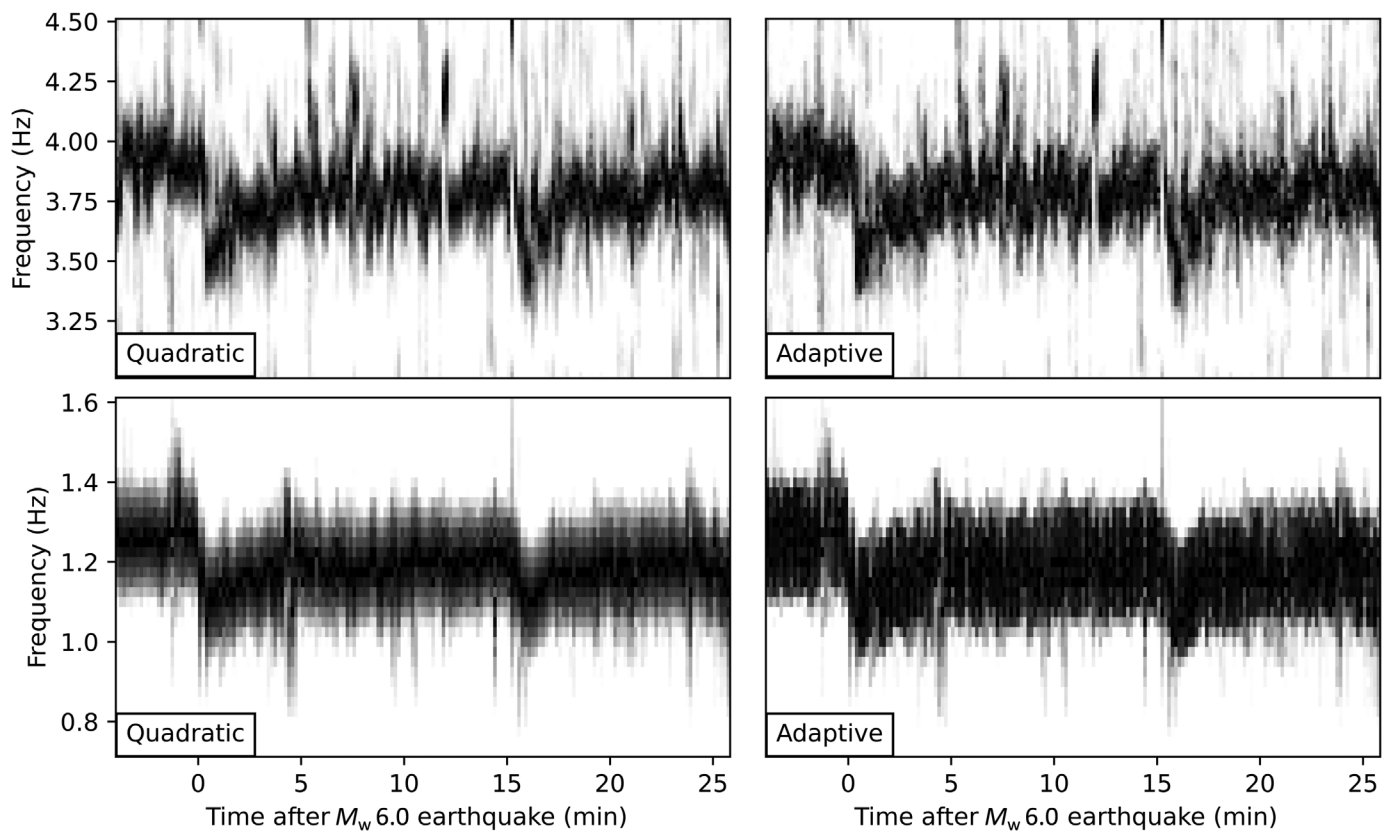
Figure 2 shows a comparison of the adaptive multitaper estimate ( $adap$ ) and the quadratic multitaper ( $qi$ ) spectrograms around two of the natural frequencies of the building at about 1.25 and 3.9 Hz. In both cases, a dramatic decrease of the natural frequencies is observed after the two largest earthquakes and the frequencies have not fully recovered after 25 min. The quadratic estimate has higher resolution (better resolved peak) than the adaptive multitaper and is best for tracking the frequency wander of the natural frequencies (Clinton *et al.*, 2006).

**Figure 1.** Time–frequency spectrogram of the  $M_w$  6.0 Mesetas earthquake recorded at a station on the 14th floor in downtown Bogota (150 km north). (a) The recorded acceleration records and (b) the corresponding spectrogram (using the quadratic multitaper) show the clear presence of at least four aftershocks including an  $M_w$  5.8 15 min later. White boxes highlight the vibrational modes of the building (see Fig. 2).

## Earthquake Source Time Functions and Spectral Ratio

Figure 3 shows the seismic records of the  $M_w$  6.0 and  $M_w$  5.8 earthquakes recorded at station PRA about 140 km from the earthquake epicenter. Two  $M_w$  4+ earthquakes are also shown that will be used as empirical Green’s functions (EGFs) to remove the effects of propagation, attenuation, and site from the estimated spectrum (Mueller, 1985; Hough, 1997; Abercrombie, 2015). The amplitude spectra of the mainshock and its EGF are also shown along with the amplitude spectrum of a noise window (for assessing the signal-to-noise ratio). A similar code as shown in pseudo-code 2 is used for estimating the amplitude spectrum, except for normalizing and taking the square root.

The spectral ratio between the mainshock and the EGF spectra is shown in Figure 4. The expected shape of such a spectral ratio has a flat spectrum at lower and higher frequencies and a transition that can be used to find the corner frequencies of the two events (Mayeda *et al.*, 2007; Agurto-Dezel *et al.*, 2017). The



spectral ratios shown have the general features expected and it is clear how the spectra of the  $M_w$  6.0 earthquake have a lower corner frequency compared with that of the  $M_w$  5.8 earthquake.

The *multitaper* also retains the phase information of the spectral estimates, and thus can estimate the transfer function and by taking its Fourier transform we obtain the source time function (STF) of the mainshock via deconvolution. Figure 4 shows the resulting STF of the  $M_w$  6.0 and  $M_w$  5.8 Mesetas earthquakes using the  $M_w$  4+ earthquakes as EGFs. The resulting STFs confirm what is observed in the spectral ratio, the duration of the  $M_w$  6.0 is greater than that of the  $M_w$  5.8 earthquake. Pseudo-code 3 can be used for obtaining the STF and spectral ratio:

#### Pseudo-code 3 – Spectral ratio and deconvolution

```
from multitaper import MTSpec, MTCross
Py1 = MTSpec(x1,nw,kspec,dt)
Py2 = MTSpec(x2,nw,kspec,dt)
# Get spectral ratio
sratio = np.sqrt(Py1.spec/Py2.spec)
# Get STF
P12 = MTCross(Py1,Py2,wl=0.001)
xcorr, dcohe, dconv = P12.mt_corr()
```

in which  $x1$ ,  $x2$  are the time series of the mainshock and aftershock, respectively. Individual spectral estimates are obtained first and later the *mtcross* module is used for calculating the

**Figure 2.** Detailed spectrograms around the vibrational modes of the building show frequency wandering (Clinton *et al.*, 2006) associated with a reduction of the stiffness of the building due to strong shaking. A reduction of the modes is around 10% after the  $M_w$  6.0 earthquakes and slightly less for the  $M_w$  5.8 earthquake. Left and right panels show the spectrogram using the quadratic and adaptive multitaper methods, highlighting the improved resolution of the quadratic multitaper, especially around the modal frequency at 1.25 Hz.

cross-spectrum in variable *P12*, a Python class that holds the cross spectrum of two series. The cross-correlation *xcorr*, normalized cross-correlation *xcohe*, and deconvolution *dconv* can be requested (in the time domain). The variable *wl* can be used for stabilizing the deconvolution with a water level. Figure 4 shows the STF from the *dconv* variable, filtered between 0.2 and 3.0 Hz.

## Coherence and Correlations of Neighboring Frequencies

Waveform similarity can be quantitatively estimated using the coherence. Previous work has shown that even for small aperture arrays waveform similarity decreases quite rapidly from high coherence at low frequencies to low coherence at higher frequencies (Vernon *et al.*, 1991; Qin *et al.*, 2019). Recent studies that use ambient noise have noticed that if the wavefield is fully diffuse, the correlation of different frequencies must be low and that detecting high correlations between distant

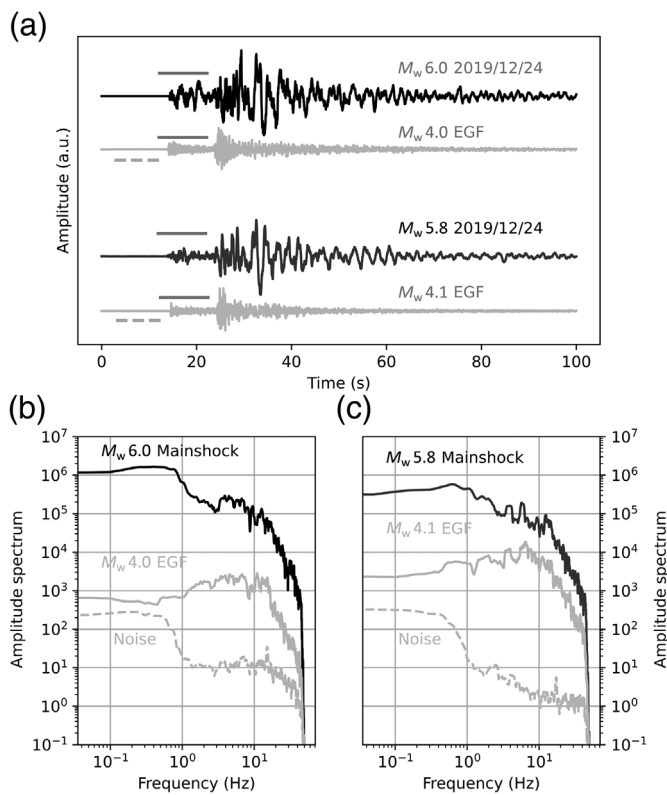


**Figure 3.** Earthquake source spectrum analysis. (a) Seismograms recorded at station PRA (140 km distance) of the  $M_w$  6.0 and  $M_w$  5.8 Mesetas earthquakes and two  $M_w$  4.0 and  $M_w$  4.1 aftershocks that are used as empirical Green's functions (EGFs). (b,c) Corresponding amplitude spectra using a 10 s window marked by the horizontal line in each seismogram.

frequencies can be used as a criterion for diffusive noise (Liu and Ben-Zion, 2016, 2018; Liu and Beroza, 2020). Using a similar idea, the coherence between distant frequencies of nonstationary signals—for example dispersive surface waves—is expected to be high (Mellors *et al.*, 1998; Prieto *et al.*, 2005). The *multitaper* allows not only estimating the coherence between two time series but also estimating the dual-frequency coherence—a matrix of correlations between the spectra at two frequencies ( $f_1$ ,  $f_2$ ). The dual-frequency coherence can be obtained for a single signal (the signal with itself) or between two signals as shown in pseudo-code 4:

#### Pseudo-code 4 – Dual-frequency coherence

```
import multitaper.utils as utils
Px = MTSpec(x,nw,kspec,dt)
Py = MTSpec(y,nw,kspec,dt)
Sx,Cx,Phx,freq = utils.df_spec(Px)
Sxy,Cxy,Phxy,freq = utils.df_spec(Px,Py)
```

in which  $Cx$  is the dual-frequency squared auto-coherence of time series  $x$  and  $Cxy$  is the dual-frequency coherence between

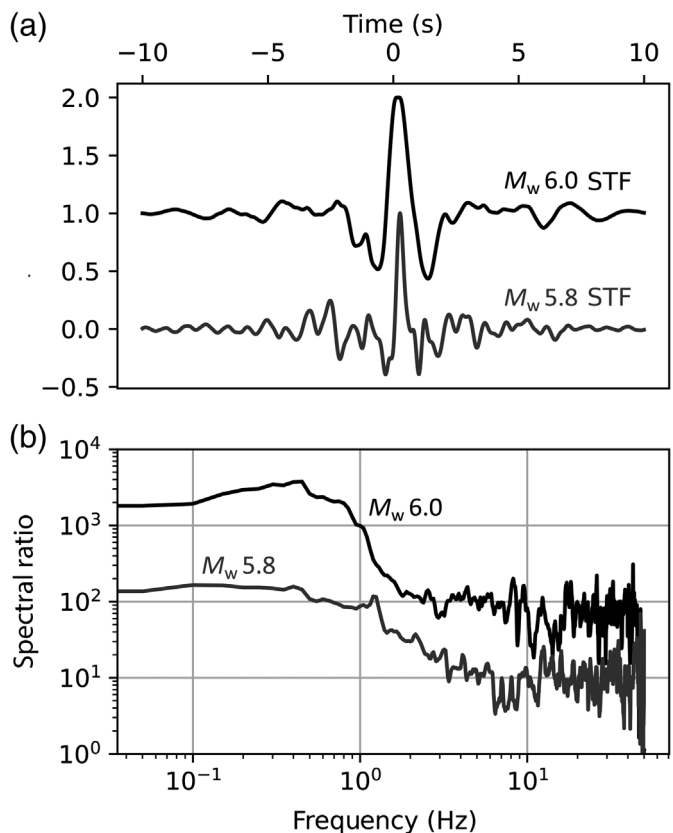


**Figure 4.** (a) Source time functions (STFs) and (b) spectral ratio of the  $M_w$  6.0 and  $M_w$  5.8 using the two  $M_w$  4 earthquakes in Figure 3 as EGFs. Note the shorter STF duration or higher corner frequency of the  $M_w$  5.8 earthquake compared with the  $M_w$  6.0 in this example.

$x$  and  $y$  series. The cross-spectrum is stored in  $Sxy$ , and the phase is stored in  $Phxy$ .

Figure 5 shows two seismic records of the  $M_w$  6.0 and  $M_w$  5.8 Mesetas earthquakes recorded at two nearby stations (VMM07 and VMM11) in a deep sedimentary basin. The two stations are separated 32 km and are about 520 km from the epicenter. For this example, I select three windows, a noise window (noise), a window with the surface wave of the  $M_w$  6.0 earthquake (mainshock), and the full trace of the  $M_w$  5.8 earthquake (aftershock). For each window, we calculate the dual-frequency coherence for a single station and between the two stations.

Figure 6 shows the resulting dual-frequency coherence for the windows selected. The auto-coherence of the noise window for station VMM07 shows low values for off-diagonal terms, whereas the mainshock and aftershock windows show significant coherence in the off-diagonal terms. For the mainshock window, the off-diagonal terms have high amplitudes between about 0.9 and 0.16 Hz, suggesting a nondiffuse dispersive wave—note the main diagonal is always 1 for auto-coherence.

The dual-frequency coherence between the two stations for the noise window shows low coherence over all frequencies,

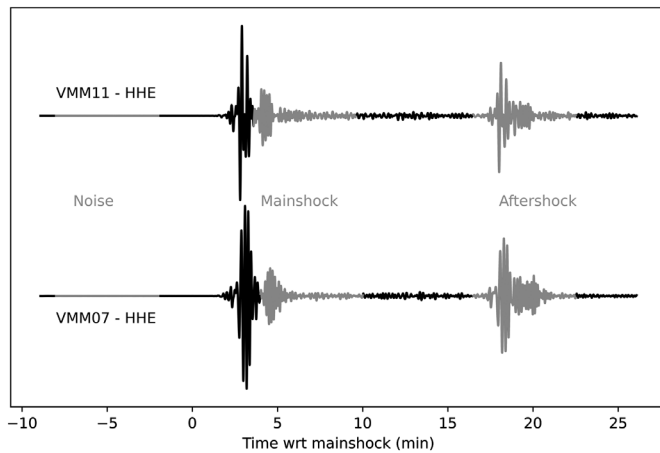


**Figure 5.** Recorded seismograms at two nearby stations (station separation 32 km and source-receiver separation 520 km). Three windows are selected for studying the correlation between neighboring frequencies using dual-frequency coherence estimates. The three windows include a noise window (noise), the surface wave of the  $M_w$  6.0 earthquake (mainshock), and the full trace of the  $M_w$  5.8 earthquake (aftershock).

confirming the diffusive nature of the wavefield. In contrast, the mainshock window shows significant coherence in the off-diagonal terms. The coherence along the main diagonal has high coherence between 0.09 and 0.12 Hz but drops rapidly at higher frequencies, whereas the off-diagonal terms have high coherence up to 0.16 Hz. The off-diagonal coherence is asymmetric with respect to the diagonal and has a different slope suggesting that the nature of the dispersion curve of the surface waves at the two stations is different.

## Conclusions

This work presents a Python package for multitaper spectral analysis. A number of examples display the different capabilities of *multitaper* for estimating the PSD, spectral ratio, and deconvolutions or dual-frequency coherencies. Other functions that include *F*-test for periodic components or application of the sine multitaper are also available and are documented in the GitHub repository. The multitaper algorithm has been widely used in geophysics, economics, medicine, climate, and of course seismology, and this contribution aims at expanding the available tools for studying the Earth.

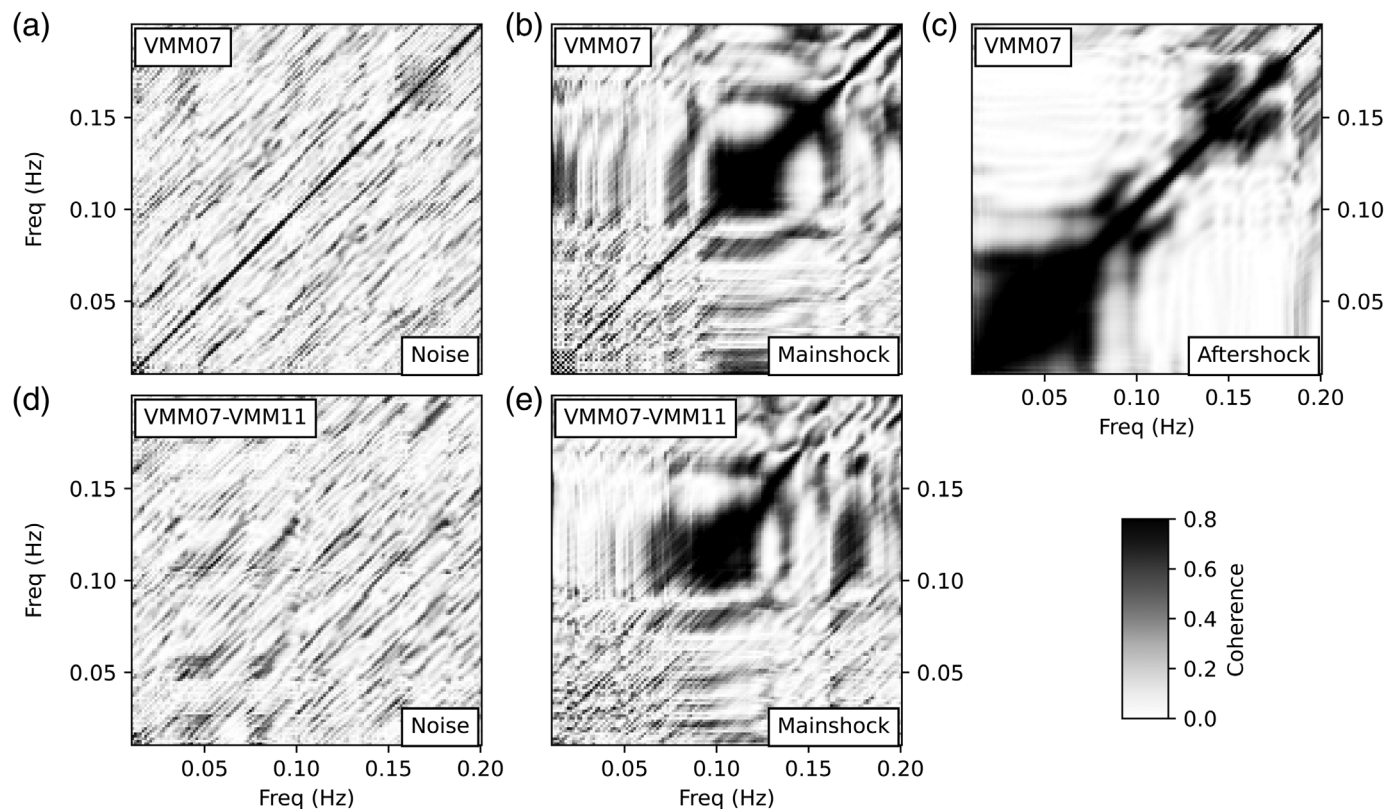


**Figure 6.** Coherence between neighboring frequencies. (a–c) The dual-frequency auto-coherence estimated from the noise, mainshock, and aftershock windows for station VMM07 and (d, e) the coherence between stations VMM07 and VMM11 for the noise and mainshock windows. Note how the coherence is low in the off-diagonal for the noise windows (diffusive noise), while for

the two other windows a higher coherence is observed in the off-diagonal. The interstation coherence for the mainshock window (surface wave) has a high correlation away from the main diagonal between 0.10 and 0.15 Hz, which can be interpreted as surface waves with distinct dispersion characteristics.

## Data and Resources

The *multitaper* package, scripts, and Jupyter Notebooks to reproduce the figures in this contribution are available on GitHub (<https://github.com/gaprieto/multitaper>). The data used here as examples come from the SGC and from a temporary deployment in the Crisanto building (Bogota) as part of a project supported by ECCI University. The SGC data are available at <http://sismo.sgc.gov.co:8080> and were downloaded using ObsPy (Beyreuther *et al.*, 2010) and the Client.get\_waveforms function. The seismic and building data used in the examples are available in a Zenodo repository (DOI: [10.5281/zenodo.6025794](https://doi.org/10.5281/zenodo.6025794)). The pymutt code is available at [code.google.com/archive/p/pymutt/](https://code.google.com/archive/p/pymutt/), and mtspec is available at [krischer.github.io/mtspec/](https://krischer.github.io/mtspec/). All websites were last accessed in June 2021.

## Declaration of Competing Interests

The author acknowledges that there are no conflicts of interest recorded.

## Acknowledgments

Special thanks to SGC and ECCI University for making the data available. The author would like to thank Pascal Audet and one anonymous reviewer who helped significantly improve user's experience for downloading, installing, and documentation access.

## References

- Abercrombie, R. E. (2015). Investigating uncertainties in empirical Green's function analysis of earthquake source parameters, *J. Geophys. Res.* **120**, no. 6, 4263–4277.
- Agurto-Detzel, H., M. Bianchi, G. A. Prieto, and M. Assumpção (2017). Earthquake source properties of a shallow induced seismic sequence in SE Brazil, *J. Geophys. Res.* **122**, no. 4, 2784–2797.
- Båth, B. M. (1974). *Spectral Analysis in Geophysics*, Elsevier, Amsterdam, The Netherlands.
- Beyreuther, M., R. Barsch, L. Krischer, T. Megies, Y. Behr, and J. Wassermann (2010). ObsPy: A Python toolbox for seismology, *Seismol. Res. Lett.* **81**, no. 3, 530–533.
- Bonilla, L. F., P. Guéguen, and Y. Ben-Zion (2019). Monitoring coseismic temporal changes of shallow material during strong ground motion with interferometry and autocorrelation, *Bull. Seismol. Soc. Am.* **109**, no. 1, 187–198.
- Bracewell, R. N. (2000). *The Fourier Transform and its Applications*, Third Ed., McGraw-Hill, New York, 616 pp.
- Chaves, E. J., S. Y. Schwartz, and R. E. Abercrombie (2020). Repeating earthquakes record fault weakening and healing in areas of megathrust postseismic slip, *Sci. Adv.* **6**, no. 32, eaaz9317.
- Clinton, J. F., S. C. Bradford, T. H. Heaton, and J. Favela (2006). The observed wander of the natural frequencies in a structure, *Bull. Seismol. Soc. Am.* **96**, no. 1, 237–257.
- Cossette, É., P. Audet, D. Schneider, and B. Grasemann (2016). Structure and anisotropy of the crust in the Cyclades, Greece, using receiver functions constrained by in situ rock textural data, *J. Geophys. Res.* **121**, no. 4, 2661–2678.
- Dannemann Dugick, F. K., S. van der Lee, G. A. Prieto, S. N. Dybing, L. Toney, and H. M. Cole (2021). ROSES: Remote online sessions for emerging seismologists, *Seismol. Res. Lett.* **92**, no. 4, 2657–2667.
- Diagourtas, D., A. Tzanis, and K. Makropoulos (2002). Comparative study of microtremor analysis methods, in *Earthquake Microzonation*, A. Roca and C. Oliveira (Editors), Birkhäuser, Basel, 2463–2479.
- Gibbons, S. J., D. B. Harris, T. Dahl-Jensen, T. Kväerna, T. B. Larsen, B. Paulsen, and P. H. Voss (2017). Locating seismicity on the Arctic plate boundary using multiple-event techniques and empirical signal processing, *Geophys. J. Int.* **211**, no. 3, 1613–1627.
- Haley, C. L., and C. J. Geoga (2020). Multitaper.jl: A Julia package for frequency domain analysis of time series, *J. Open Sour. Softw.* **5**, no. 55, 2463.
- Häusler, M., C. Michel, J. Burjánek, and D. Fäh (2021). Monitoring the Preonzo rock slope instability using resonance mode analysis, *J. Geophys. Res.* **126**, no. 4, e2020JF005709.
- Hough, S. E. (1997). Empirical Green's function analysis: Taking the next step, *J. Geophys. Res.* **102**, no. B3, 5369–5384.
- Jaimes, N., G. A. Prieto, and C. Rodriguez (2022). Detection of building response changes using deconvolution interferometry: A case study in Bogota, Colombia, *Seismol. Res. Lett.* **93**, no. 2A, 931–942, doi: [10.1785/0220210219](https://doi.org/10.1785/0220210219).
- Jang, H., Y. Kim, H. Lim, and R. W. Clayton (2019). Seismic attenuation structure of southern Peruvian subduction system, *Tectonophysics* **771**, 228203.
- Kay, S. M., and S. L. Marple (1981). Spectrum analysis—A modern perspective, *Proc. IEEE* **69**, no. 11, 1380–1419.
- Kemna, K. B., A. F. Peña Castro, R. M. Harrington, and E. S. Cochran (2020). Using a large-n seismic array to explore the robustness of spectral estimations, *Geophys. Res. Lett.* **47**, no. 21, e2020GL089342.
- Kong, Q., R. M. Allen, M. D. Kohler, T. H. Heaton, and J. Bunn (2018). Structural health monitoring of buildings using smart-phone sensors, *Seismol. Res. Lett.* **89**, no. 2A, 594–602.
- Larsen, Y., and A. Hanssen (2004). Dual-frequency dual-wavenumber cross-coherence of nonstationary and inhomogeneous harmonizable random fields, *Proc. IEEE Int. Conf. Acoust., Speech, Signal Process.*, Montreal, QC, Canada, IEEE, II-625–II-628.
- Lees, J. M., and J. Park (1995). Multiple-taper spectral analysis: A stand-alone C-subroutine, *Comput. Geosci.* **21**, no. 2, 199–236.
- Liu, X., and Y. Ben-Zion (2016). Estimating correlations of neighboring frequencies in ambient seismic noise, *Geophys. J. Int.* **206**, no. 2, 1065–1075.
- Liu, X., and Y. Ben-Zion (2018). Analysis of non-diffuse characteristics of the seismic noise field in southern California based on correlations of neighboring frequencies, *Geophys. J. Int.* **212**, no. 2, 798–806.
- Liu, X., and G. C. Beroza (2020). Quantifying the effects of nondiffuse noise on ballistic and coda wave amplitude from variances of seismic noise interferometry in Southern California, *J. Geophys. Res.* **125**, no. 1, e2019JB017617.
- Liu, Z., J. Park, and S. I. Karato (2018). Seismic evidence for water transport out of the mantle transition zone beneath the European Alps, *Earth Planet. Sci. Lett.* **482**, 93–104.
- Madariaga, R., S. Ruiz, E. Rivera, F. Leyton, and J. C. Baez (2019). Near-field spectra of large earthquakes, *Pure Appl. Geophys.* **176**, no. 3, 983–1001.
- Mayedá, K., L. Malagnini, and W. R. Walter (2007). A new spectral ratio method using narrow band coda envelopes: Evidence for

- non-self-similarity in the Hector Mine sequence, *Geophys. Res. Lett.* **34**, no. 11, doi: [10.1029/2007GL030041](https://doi.org/10.1029/2007GL030041).
- Mayorga, E., V. Dionicio, M. Lizarazo, P. Pedraza, E. Poveda, O. Mercado, D. Siervo, L. Aguirre, R. Bolaños, F. Garzón, *et al.* (2020). *EL SISMO DE MESETAS, META DEL 24 DE DICIEMBRE DE 2019 Aspectos sismológicos, movimiento fuerte y consideraciones geodésicas*, Servicio Geológico Colombiano (link), Bogotá.
- Melgar, D., B. W. Crowell, T. I. Melbourne, W. Szeliga, M. Santillan, and C. Scrivner (2020a). Noise characteristics of operational real-time high-rate GNSS positions in a large aperture network, *J. Geophys. Res.* **125**, no. 7, e2019JB019197.
- Melgar, D., T. I. Melbourne, B. W. Crowell, J. Geng, W. Szeliga, C. Scrivner, M. Santillan, and D. E. Goldberg (2020b). Real-time high-rate GNSS displacements: Performance demonstration during the 2019 Ridgecrest, California, earthquakes, *Seismol. Res. Lett.* **91**, no. 4, 1943–1951.
- Mellors, R. J., F. L. Vernon, and D. J. Thomson (1998). Detection of dispersive signals using multitaper dual-frequency coherence, *Geophys. J. Int.* **135**, no. 1, 146–154.
- Morelli, A., L. Zaccarelli, A. Cavaliere, and R. M. Azzara (2021). Normal modes of a medieval tower excited by ambient vibrations in an urban environment, *Seismol. Res. Lett.* **93**, no. 1, 315–327.
- Mueller, C. S. (1985). Source pulse enhancement by deconvolution of an empirical Green's function, *Geophys. Res. Lett.* **12**, no. 1, 33–36.
- Noriega-Londoño, S., M. A. Bermúdez, S. A. -MorenoRestrepo, M. I. Marín-Cerón, and H. -DelgadoGarcía, 2021, Earthquake ground deformation using DInSAR analysis and instrumental seismicity: The 2019 M 6.0 Mesetas earthquake, Meta, Colombian Andes, *Boletín de la Sociedad Geológica Mexicana* **73**, no. 2, doi: [10.18268/BSGM2021v73n2a090221](https://doi.org/10.18268/BSGM2021v73n2a090221).
- Olafsson, S., and R. Sigbjörnsson (1995). Application of ARMA models to estimate earthquake ground motion and structural response, *Earthq. Eng. Struct. Dynam.* **24**, no. 7, 951–966.
- Pardo-Igúzquiza, E., M. Chica-Olmo, and F. J. Rodríguez-Tovar (1994). CYSTRATI: A computer program for spectral analysis of stratigraphic successions, *Comput. Geosci.* **20**, no. 4, 511–584.
- Percival, D. B., and A. T. Walden (1993). *Spectral Analysis for Physical Applications*, Cambridge University Press, Cambridge, United Kingdom.
- Prieto, G., R. Parker, and F. Vernon (2009). A Fortran 90 library for multitaper spectrum analysis, *Comput. Geosci.* **35**, 1701–1710.
- Prieto, G. A., R. L. Parker, D. J. Thomson, F. L. Vernon, and R. L. Graham (2007). Reducing the bias of multitaper spectrum estimates, *Geophys. J. Int.* **171**, no. 3, 1269–1281.
- Prieto, G. A., F. L. Vernon, G. Masters, and D. J. Thomson (2005). Multitaper Wigner-Ville spectrum for detecting dispersive signals from earthquake records, *Conf. Record of the Thirty-Ninth Asilomar Conf. Signals, Systems and Computers, 2005*, IEEE, 938–941.
- Qin, L., F. L. Vernon, C. W. Johnson, and Y. Ben-Zion (2019). Spectral characteristics of daily to seasonal ground motion at the Piñon flats observatory from coherence of seismic data, *Bull. Seismol. Soc. Am.* **109**, no. 5, 1948–1967.
- Rahim, K. J., W. S. Burr, and D. J. Thomson (2014). Applications of multitaper spectral analysis to nonstationary data, *Ph.D. Thesis*, Queen's University, R package version 1.0-15, available at <https://CRAN.R-project.org/package=multitaper> (last accessed June 2021).
- Tary, J. B., R. H. Herrera, J. Han, and M. van der Baan (2014). Spectral estimation—What is new? What is next? *Rev. Geophys.* **52**, no. 4, 723–749.
- Thomson, D. J. (1982). Spectrum estimation and harmonic analysis, *Proc. IEEE* **70**, no. 9, 1055–1096.
- Thomson, D. J., and F. L. Vernon (1998). Signal extraction via multitaper spectra of non-stationary data, *Proc. Thirty-Second Asilomar Conf. on Signals, Systems and Computers*, Madison, Wisconsin, IEEE, 271–275, Omnipress.
- Trugman, D. T., and A. Savvaidis (2021). Source spectral properties of earthquakes in the Delaware basin of West Texas, *Seismol. Res. Lett.* **92**, no. 4, 2477–2489.
- Ugalde, A., J. J. Egozcue, and C. R. Ranero (2021). A new autoregressive moving average modeling of H/V spectral ratios to estimate the ground resonance frequency, *Eng. Geol.* **280**, 105957.
- Vernon, F. L., J. Fletcher, L. Carroll, A. Chave, and E. Sembera (1991). Coherence of seismic body waves from local events as measured by a small-aperture array, *J. Geophys. Res.* **96**, no. B7, 11,981–11,996.

---

Manuscript received 22 November 2021

Published online 29 March 2022